DOI 10.1007/s11595-012-0397-3

Microstructure and Mechanical Properties of an *in situ* Synthesized TiB and TiC Reinforced Titanium Matrix Composite Coating

LI Jun, YU Zhishui, WANG Huiping, LI Manping

(School of Materials Engineering, Shanghai University of Engineering Science, Shanghai 201620, China)

Abstract: A titanium-based composite coating reinforced by *in situ* synthesized TiB and TiC particles was fabricated on Ti6Al4V by laser cladding. The microstructure and mechanical properties were investigated. The coating was mainly composed of α-Ti cellular dendrites and an eutectic in which a large number of rod/needle-shaped TiB and a few equiaxial TiC particles were homogeneously embedded. The microstructural evolution could be divided into four stages: precipitation and growth of primary β-Ti phase, formation of the binary eutectic β-Ti+TiB, formation of the ternary eutectic β-Ti+TiB+TiC, and solid transformation from β-Ti to α-Ti. Microhardness of the coating showed a gradient variation from the surface (about $HV_{0.2}$ 876) to the bottom (about $HV_{0.2}$ 660) and was prominently improved in comparison with that of the substrate. Fracture toughness of the coating also exhibited a gradient variation from the surface (6.3 MPa•$m^{1/2}$) to the interface (11.9 MPa•$m^{1/2}$). Wear resistance of the coating was significantly superior to that of Ti6Al4V.

Key words: coating; laser cladding; *in situ* synthesis; microstructure; mechanical properties

1 Introduction

Titanium alloys are widely used in aerospace, chemical, petrochemical and marine industries as key structural components due to their combination of high strength weight ratio, excellent corrosion resistance, and superior mechanical properties at elevated temperatures[1]. However, titanium alloys exhibit a number of poor tribological properties, such as high and unstable friction coefficient, low adhesive, abrasive and fretting wear resistance, and difficulties in lubrication, which restrict their potential applications as substitutes for tribological components conventionally made of steel[2].

Wear is a surface-dependent property. Wear resistance can be improved by appropriately tailoring surface microstructure and/or composition, *i e*, by modifying the surface without affecting the bulk[3]. Many surface modification techniques are available, including ion implantation, physical and chemical vapor deposition processes, plasma spraying, and laser cladding. Of these, laser cladding has a number of attractive advantages, such as low and precise heat input, small heat-affected zone, high processing speed and productivity, low residual stress and distortion, possible elimination of pre- and post-repair heat treatments, high dimensional accuracy, and great process flexibility and reliability, which allow unique mechanical and chemical properties to be imparted to a surface without affecting the bulk[4,5]. In recent years, laser cladding of ceramic-metal composite coatings onto Ti-alloy substrates has been used to improve the surface properties of titanium alloys. Ceramic phases such as WC[6-8], TiN[9-11], TiC[12-14], Ti_3Al[15], TiB[16, 17], SiC[18], ZrO_2[19] and Al_2O_3[20] have been directly added into coatings or *in situ* synthesized by reacting pure elements during laser cladding. Comparatively, the *in situ* synthesized reinforcements may be more compatible with the matrix and the interface may be cleaner, which ensures that the matrix has sufficient strength to transfer stress. Among *in situ* synthesized reinforcements, TiC and TiB have been extensively regarded as the two best reinforcements in a titanium matrix, for a number of reasons, including their high elastic modulus, their similar density to Ti alloys, and their excellent interfacial bonding with titanium

(Received: June 26, 2010; Accepted: Aug. 29, 2011)

LI Jun(李军): Prof.; Ph D; E-mail: jacob_lijun@sina.com

Funded by the the National Natural Science Foundation of China (No. 51002093), the Shanghai Science and Technology Development Foundation, China (No. 08QA14035) and the Shanghai Leading Academic Discipline Project, China (No. J51402)

matrixes[21-23]. The use of titanium matrix composite coatings reinforced by TiB and TiC has produced titanium alloys with increased stiffness, enhanced temperature strength, good creep performance, and increased fatigue and wear resistance, thus widening their utilization fields[17].

Current methods for fabrication of *in situ* synthesized TiB-TiC reinforced titanium matrix composites usually rely on techniques such as ingot metallurgy (IM)[24-30], self-propagation high-temperature synthesis (SHS)[31] or powder metallurgy (PM)[21, 32], *etc*, which are rather complex and may result in material waste and increased costs. Few studies have investigated laser cladding as a means of preparing titanium matrix composite coatings[33] and have focused mainly on microstructural characterizations, with little detailed discussion regarding the microstructural evolution of the coating or the interface. Comprehensive investigation of the mechanical properties is lacking, especially regarding the wear behavior and the distribution of fracture toughness in cross sections of the coatings.

As an extension of previous investigations, the aim of the present work was to improve the hardness and wear resistance of a Ti6Al4V substrate by laser cladding a TiC-TiB reinforced titanium matrix composite coating onto its surface. A detailed investigation into the microstructure, phase and mechanical properties (in terms of microhardness, fracture toughness and wear resistance) was undertaken. The possible mechanism underlying the microstructural evolution of the TiB and TiC reinforcements is discussed.

2 Experimental

A Ti6Al4V alloy with a composition of 6.5 wt% Al, 4.26 wt% V and the balance Ti was used as a substrate material. It was hot rolled and annealed in the $\alpha+\beta$ range, and was machined into cylinders 50 mm in diameter and 10 mm long. The substrate surface was polished with 200-grit SiC abrasive paper and degreased in acetone prior to coating. The powder mixture of the coating alloy contained pure titanium (87 wt%), B_4C (9 wt%) and Al (4 wt%). This was mixed with a binder (4% polyvinyl alcohol, PVA) to form a slurry, which was applied to the Ti6Al4V to form a layer of 0.8-1.0 mm thickness and allowed to dry for 5 h at 90 ℃.

Laser cladding was carried out using a 5-kW continuous wave CO_2 gas laser with an applied power (P) of 3-3.5 kW, beam diameter (D) of 4 mm and scanning speed (v) of 5 mm/s. These laser parameters had been optimized by ensuring a good interface fusion, a smooth coating surface, and a minimum dilution. The molten pool was shielded from heavy oxidation by blowing high purity nitrogen gas over the surface during laser treatment. Eight overlap tracks were clad side by side, with a overlap ratio of approximately 25%, in order to clad the entire 30×30 mm surface of the substrate specimen for the subsequent friction and wear test.

Phase constituents of the coating were analyzed by a Rigaku D/mas 2550V X-ray Diffractometer (XRD) with Cukα radiation. Microstructural characterization was carried out with a VHX-600K Optical Microscope (OM), a JSM6460 Scanning Electron Microscope (SEM) and an INCN Electron Probe Micro Analyzer (EPMA). The cross section of the sample was prepared on a Buehler Phoenix 4000 sample preparation system and then rinsed with alcohol and acetone. A mixture of 20 vol% HF and 80 vol% HNO_3 was used as the etchant.

Microhardness measurement was performed on a HXD-1000TM microhardness tester with a load of 200 g applied for 15 s. Dry sliding friction and wear tests without lubricant were carried out using the pin-on-disc mode on a HT-500 friction and wear apparatus at room temperature. The discs of the coating and Ti6Al4V were polished with 200-grit SiC abrasive paper prior to the wear test, and the layer was removed to about 200 μm. Counter-body pins made of 45# steel with a hardness of HRC 35 and a surface roughness of Ra=0.4 μm were machined in the form of cylinders 5 mm in diameter and 24 mm long. The applied load was 17.5 N. The sliding speed was kept constant at 0.176 m/s. The total sliding time was 600 min. The appearance of the worn surfaces of the coating and Ti6Al4V was observed using a VHX-600K Optical Microscope (OM), and phase constituents of worn scraps were identified using a Rigaku D/mas 2550V X-ray Diffractometer (XRD). Fracture toughness of the coating was measured by the Vickers indentation method and calculated by the following equation:

$$\frac{K_{1C}}{Ha^{1/2}}=0.203\left(\frac{c}{a}\right)^{-3/2} \quad (1)$$

in which K_{1C} is fracture toughness, MPa•m$^{1/2}$; H is the Vickers hardness, MPa; a is half length of the diagonal line of an indentation, m; c is half length of cracks, m.

3 Results and discussion

3.1 XRD analyses

Phase constituents of the coating were identified from the X-ray diffraction spectrum shown in Fig.1. According to the indexed results of the diffraction peaks in terms of PDF, the coating mainly included α-Ti as the matrix, in which a certain amount of elements such as Al and C were dissolved, along with a few TiB and TiC as the reinforcements. TiB and TiC were new phases that were *in situ* synthesized between Ti and B_4C in the coating during laser cladding. No B_4C phase was observed, which meant that the reactions between Ti and B_4C consumed all of the B_4C powder. The following reactions between Ti and B_4C may take place:

$$5Ti+B_4C=4TiB+TiC \quad (1)$$

$$3Ti+B_4C=2TiB_2+TiC \quad (2)$$

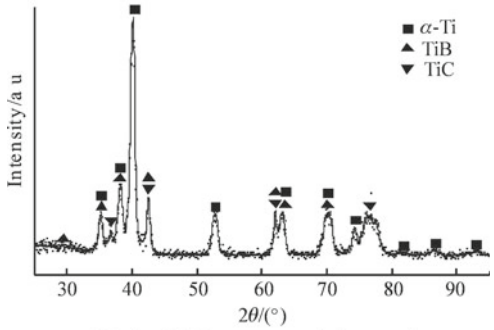

Fig.1 XRD pattern of the coating

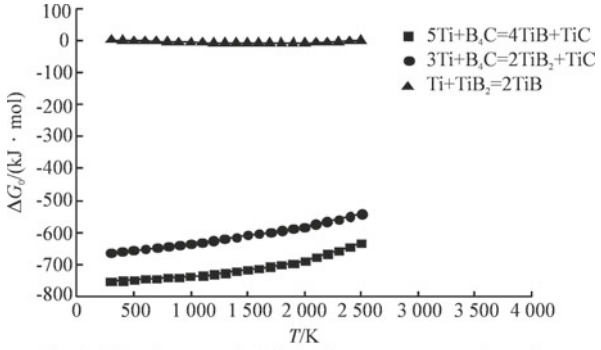

Fig.2 The changes in Gibbs free energy as a function of temperature for the Reactions (1)-(3)

The changes in Gibbs free energy of the above reactions were calculated using the thermodynamic data from Reference[34]. As shown in Fig.2, the ΔG_o of both reactions is negative up to 2 500 K, which indicates that both reactions can spontaneously occur, namely, TiB_2, TiB and TiC can be formed. At the same temperature, the spontaneous chemical reactions followed the order: (1)>(2), so that TiB can be formed in preference to TiB_2. However, no TiB_2 was observed in the XRD analyses results, which could be attributed to the excess of titanium in this system. *In situ* synthesized TiB_2 will simultaneously react with the titanium matrix by the following reaction:

$$Ti+TiB_2=2TiB \quad (3)$$

As shown in Fig.2, the thermodynamic calculation result reveals that this reaction can also spontaneously occur, although the ΔG_o is less negative. Based on the above analyses, TiB and TiC reinforcements can be *in situ* synthesized in the present system, in accordance with the XRD analysis results.

3.2 Microstructural characterizations

An SEM overview of the TiB+TiC/Ti composite coating is depicted in Fig.3, and clearly reveals that the microstructure of the coating involves the morphologies of TiB and TiC phases. The microstructure of the coating was very uniform and was mainly composed of coarse primary cellular dendrites (C1) and the eutectic transformation product, in which a large number of coarse rod-shaped (C2), needle-shaped (C3) and fine needle-shaped particles (C4) and a few equiaxial particles (C5) were homogeneously embedded. Combined with the corresponding micro composition analyses, *i e*, EPMA and the XRD analysis results, the phases with different morphologies were identified. Coarse cellular dendrites were α-Ti, and equiaxial particles were TiC with a mean size of 0.5 μm. The TiB phase presented three morphologies: a coarse rod shape and needle shape with a mean diameter of 1 μm and a typical length of 30 μm, and a fine needle shape with a mean diameter of 0.4 μm and a typical length 4 μm. The TiC and fine needle-shaped TiB particles were distributed within the interdendritic zone. For coarse TiB particles, one part was located within the interdendritic zone, the other part was surrounded by coarse cellular dendrites. Comparatively, the amount of TiB was far higher than that of TiC, which was also validated by the XRD results. The difference in amount was mostly correlated with the initial composition ratio of B and C (about 4:1 in molar ratio). Dissolution of C into the titanium matrix (B almost has no dissolution in the titanium matrix) further reduced the final content of TiC, to a certain extent.

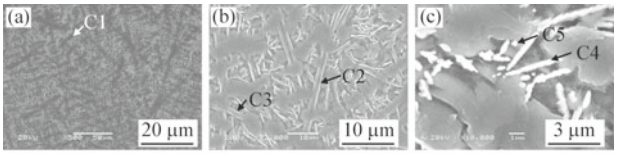

Fig.3 SEM images of the coating in cross section (a) microstructure of the coating at low magnification; (b) and (c) microstructure of the coating at high magnification

Differences in morphology between TiB and TiC could be primarily related to differences in their crystal structures. TiC has a B1 crystal structure, where the unit cell is completely symmetrical without a preferential growth crystal facet, no matter what the geometric configuration and chemical bonding may be. This causes TiC to grow in an equiaxial or near-equiaxial shape when TiC is precipitated by the binary eutectic reaction[32]. The reactant TiB has a B27 prismatic structure with lattice parameters a=/0.612 nm, b=0.306 nm, and c=/0.456 nm. It grows preferably along the [010] crystal direction for the occupation of atoms and chemical bonds is asymmetrical[35].

The concrete difference in morphology of the reinforcements can be rationalized by the microstructural evolution progress. The growth mechanism of reinforcements can be divided into a diffusion mechanism and a dissolution precipitation mechanism according to the processing temperature. When the temperature is lower than that related to the liquid phase line, reinforcements are *in situ* synthesized by a diffusion mechanism. In contrast, a dissolution precipitation mechanism will play a key role in formation of reinforcements. In this research, the heat exerted on the molten pool is comparatively high due to the high laser power of 3.5 kW. In addition, reactions (1) and (2) will release a great amount of heat, which has been confirmed by many researchers[35, 36]. Overlap of these two heat inputs will result in a drastic enhancement of temperature and will cause the *in situ* synthesized TiB and TiC to melt into the liquid titanium during fabrication. During the subsequent cooling, TiB and TiC will nucleate and grow from the liquid phase. According to the projection of the liquidus surface in the Ti-B-C ternary phase diagram[37], the composition of the powder mixtures is located at the rich-titanium corner, in which a ternary eutectic reaction $L \Leftrightarrow \beta\text{-Ti} + \text{TiB} + \text{TiC}$ and three binary eutectic reactions corresponding to $L \Leftrightarrow \beta\text{-Ti} + \text{TiB}$, and $L \Leftrightarrow \text{TiB} + \text{TiC}$ are present. Combined with the analysis of the Ti-B-C phase diagram and the observation of the coating microstructure, the microstructural evolution process can be described as follows:

Precipitation and growth of primary phase β-Ti. TiB and TiC were *in situ* synthesized and melted into the liquid phase as described above. In the subsequent cooling process, primary phase β-Ti will nucleate from the liquid phase by the reaction $L \Leftrightarrow \beta\text{-Ti}_p + \text{L}_p$ and grow into the coarse cellular or dendritic shapes, due to sufficient time and space to grow in the liquid alloy.

Formation of the binary eutectic of β-Ti and TiB. As the temperature was gradually reduced, one part of the liquid phase was further transformed into β-Ti and TiB by the binary reaction $L_p \Leftrightarrow (\beta\text{-Ti} + \text{TiB})_e + L_e$. β-Ti and TiB will grow quickly owing to rapid atom diffusion in the liquid phase. β-Ti may collide with TiB growing preferably along the [010] crystal direction and will grow around the surface of the TiB. As a result, coarse rod-shaped and needle-shaped TiB particles are surrounded by β-Ti, as shown in Fig.3 (b).

Formation of the ternary eutectic of β-Ti, TiB and TiC. With a further decrease in temperature, the remaining liquid phase will be crystallized into three kinds of phases corresponding to β-Ti, fine needle-shaped TiB and equiaxial TiC particles by the ternary eutectic reaction $L_e \Leftrightarrow (\beta\text{-Ti} + \text{TiB} + \text{TiC})_e$. Owing to the fast reaction time and slow atom diffusion rate in the solid state, TiB and TiC are very fine in comparison with primary β-Ti and the binary eutectic product TiB.

Formation of α-Ti. β-Ti will be transformed into α-Ti by the following allotropic transformation reaction: $\beta\text{-}Ti \Leftrightarrow \alpha\text{-Ti}$. The α-Ti, TiB and TiC are then maintained at room temperature.

3.3 Mechanical properties

Microhardness measurements were performed to acquire a general understanding of microhardness distribution across the coating. As shown in Fig.4, the profile can be divided into three regions, corresponding to the coating, the dilution zone (DZ), and the substrate. Microhardness ranged from HV 875.64 to HV 659.75 in the coating and presented a gradient distribution. In the dilution zone, microhardness exhibited a variation from HV 603.4 to HV 353 and gradually decreased with increasing distance from the coating surface. For the substrate, the constant microhardness of about HV 330 was obtained. Compared with the substrate, the microhardness of the coating was prominently enhanced, which was the mutual result of the grain-refinement hardening and dispersion hardening of TiB and TiC phases. The microhardness distribution characteristics of the coating were relevant to the convection movement of the melt and the relative densities of constituent elements.

The *in situ* synthesized TiB and TiC were dissolved in the liquid phase. The C and B atoms tend to float upwards in the molten pool owing to their relatively low densities in comparison with that of the titanium matrix. During the subsequent solidification, the amount of TiB and TiC is gradually reduced with increasing distance from the surface of the coating, and

presents a gradient distribution on a macroscale. This particle movement driven by differential density was also reported in previous studies[38], where the particles tended to move toward the upper regions in a particle-reinforced MMC layer. Additionally, the convective flow in the liquid will have an effect on the movement of the ceramic particulates. The forces and flow patterns resulting from surface tension gradients will undoubtedly strongly influence the distribution of ultra-fine ceramic reinforcements *in situ* formed[39].

Fracture toughness of the coating was measured by the Vickers indentation method. OM images of Vickers indentations obtained at different positions from the cross section of the coating, including upper, middle, bottom and interface parts are indicated in Fig.5. All indentations are very clear and integral, except for some fine cracks that were generated at four corner angles of the indentations and propagated towards the area far from the indentations. When a load was applied to the cross section of the coating, deformation disaccord occurred between reinforcements and the matrix due to their significant differences in modulus elasticity (modulus elasticities of α-Ti, TiB and TiC are 115, 550 and 440 GPa, respectively). As a result, the interface between reinforcements and the matrix gives rise to the stress concentration and cracks are easily generated and propagated. Cracks located at different positions presented different morphologies.

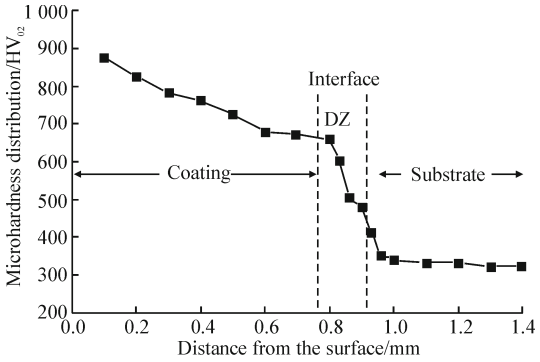

Fig.4 Microhardness of the coating with distance from the surface

With the increase in distance from the surface, propagation distance of cracks is gradually reduced, which indicates that fracture toughness is correspondingly increased. The calculation results of fracture toughness also further substantiate the above analysis. Fracture toughness of the upper, middle, bottom and interface of the coating were 6.328, 8.913, 11.940 and 11.928 MPa•m$^{1/2}$, respectively, and exhibited a gradient distribution. This variation tendency was exactly contrary to the microhardness

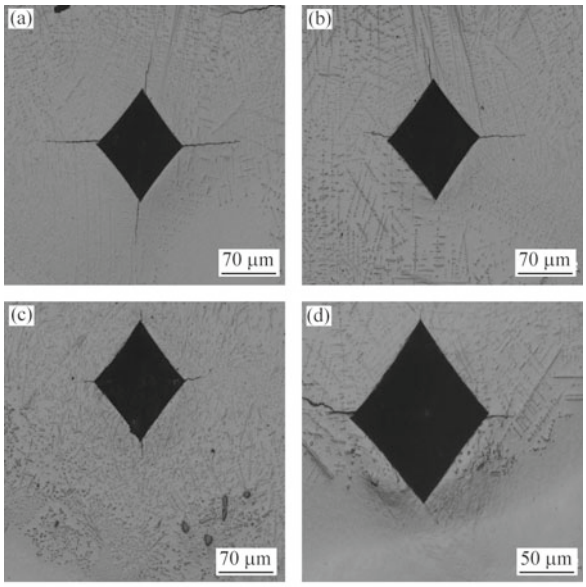

Fig.5 OM morphologies of the impressions obtained at different positions from the cross section of the coating: (a) upper; (b) middle; (c) bottom; and (d) interface

distribution, which can be adequately explained by the distribution of TiB and TiC reinforcements.

Fig.6 shows the changes in friction coefficient of the coating and Ti6Al4V with sliding time. For the coating, friction coefficient ranged from 0.150 to 0.571, with an average value of about 0.452. The friction coefficient of Ti6Al4V presented a change from 0.291 to 0.658, with an average value of about 0.586, which was higher than that of the coating. At the initial wear stage, the friction coefficient for the coating and Ti6Al4V drastically fluctuated with the changes in time, indicating that wear mainly takes place at some protruding portions of the pin and disks. The friction coefficient gradually stabilized 90 min later, which meant that wear occurred on the entire surface of pin and disks.

The worn surface appearance of Ti6Al4V and the coating is shown in Fig.7. A great number of plough grooves with different widths and depths were observed on the worn surface of Ti6Al4V, confirming that the wear process of Ti6Al4V was governed by the effect of a micro-cutting mechanism. The plough grooves were contaminated by many fine bay worn scraps. Some were uniformly dispersed in grooves, and others assemble together to form flakes. The worn surface morphology of the coating presented significantly different characteristics. The entire worn surface was covered with bay worn scraps except for an occasional portion of the zone and a few grooves of small depth. In order to further investigate the wearing mechanism of the coating, phase continents of worn scraps as the

wear product between the coating and 45# steel were identified by XRD. As shown in Fig.8, worn scraps are composed of a great amount of Fe_2O_3 and little Fe, which confirms that many of the bay worn scraps adhering to the coating surface should be Fe_2O_3.

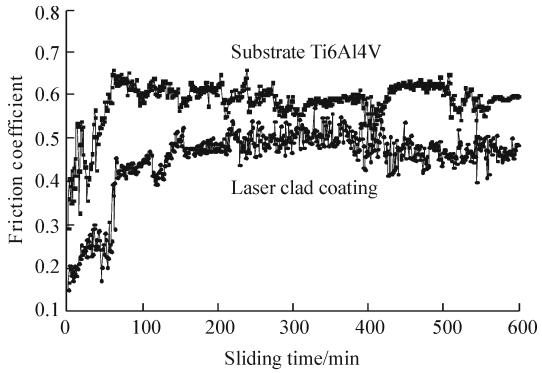

Fig.6 The changes in friction coefficient of Ti6Al4V and the coating with sliding time

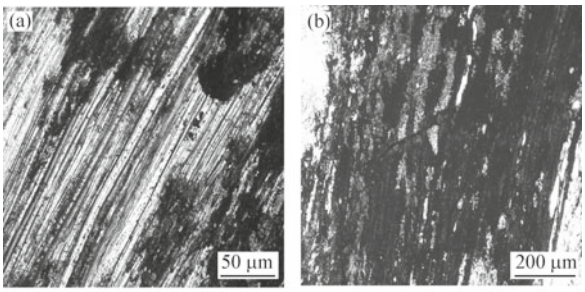

Fig.7 OM images of the initial worn surface of Ti6Al4V and the coating: (a) Ti6Al4V; (b) the coating

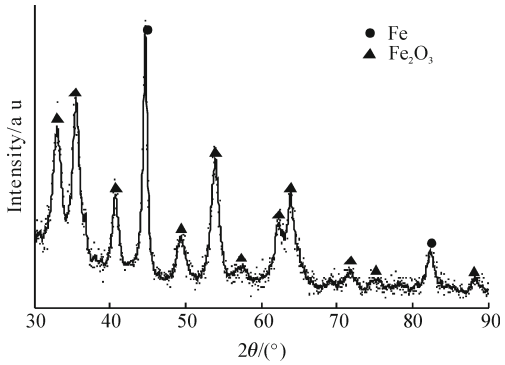

Fig.8 XRD pattern of wear scraps as the wear product of the coating and 45# steel

At the initial sliding stage, the softer matrix would wear out faster compared to the hard reinforcements and the reinforcements will then protrude over the worn surface, protecting the coating from being further worn away and producing the micro-cutting effect on the surface of 45# steel. Many 45# steel scraps were peeled off of the surface of 45# steel and adhered to the surface of the coating. The protuberant reinforcements may be fractured due to the dual effects of the reduction in support by the matrix and the effective load exerted on each individual reinforcement. At the subsequent sliding process, wear mainly takes place between 45 # steel and 45# steel scraps. Heat resulting from friction would make the major element Fe of scraps react with O_2 by the following possible reactions:

$$2Fe+O_2=2FeO \quad (4)$$

$$4Fe+3O_2=2Fe_2O_3 \quad (5)$$

$$3Fe+2O_2=Fe_3O_4 \quad (6)$$

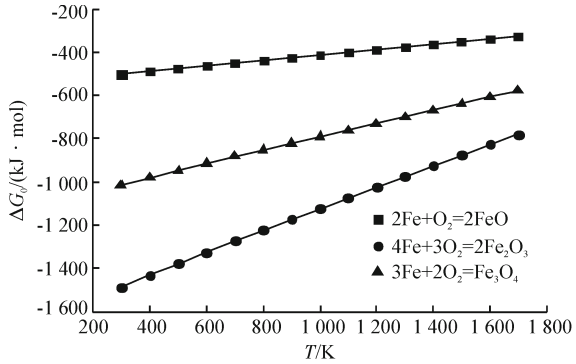

Fig.9 The changes in Gibbs free energy as a function of temperature for Reactions (4)-(6)

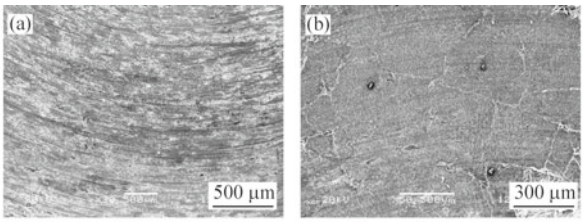

Fig.10 SEM images of the worn surface of Ti6Al4V and the coating dealt with by 10 vol% Hcl: (a) Ti6Al4V; (b) the coating

The changes in Gibbs free energy as a function of temperature of the above reactions were calculated. As shown in Fig.9, the ΔG_o of the three reactions is negative across the entire temperature range from 298 K to 1 700 K, which means that three reactions can spontaneously occur; namely, FeO, Fe_2O_3 and Fe_3O_4 can be formed. However, reaction (5) can take place prior to reactions (4) and (6) at the same temperature. That is to say, Fe_2O_3 can be formed in preference to FeO and Fe_3O_4, which is in accordance with the analysis result of XRD. Many scraps mainly consisting of Fe_2O_3 will further aggravate the wear of 45# steel. Although Fe_2O_3 scraps can have a micro-cutting effect on the coating surface, the damage to the coating is negligible due to the high microhardness of the coating in comparison with that of scraps, which is verified by XRD analysis results. As shown in Fig.9, no titanium, TiB or TiC are found, indicating that the amount of phases peeled off the coating is so small that they cannot be identified by XRD. In order to observe the ture worn surface morphology of Ti6Al4V and the coating, 10 vol% HCl was used as the etchant to remove the layer consisting

of Fe_2O_3 and Fe. SEM examination results are shown in Fig.10. It reveals clearly that a great amount of grooves and abrasion are distributed on the whole worn surface of Ti6Al4V. Comparatively, it is surprising that the worn surface of the coating presents a very smooth and clean morphology on a macroscale.

These analyses reveal that wear resistance of the coating is strongly enhanced due to the combination of unique physical, mechanical and chemical properties of TiB and TiC reinforcements uniformly distributed in the matrix. TiB and TiC with B27 and B1 crystal structures, respectively, possess very high melting points and strong atomic bonds, which offer the coating excellent abrasive wear resistance due to their outstanding resistance to micro-cutting and plowing during dry sliding wear processes. On the other hand, a titanium matrix with some ductility and toughness can release the stress exerted on the coating by plastic deformation, which also contributes to the improved wear resistance of the coating by preventing the coating from micro-cracking and micro-fracturing to a certain extent. The rapidly solidified fine microstructure having improved combination of strength and toughness also makes some positive contribution to the outstanding wear resistance of the coating.

4 Conclusions

In situ synthesized TiB+TiC reinforced titanium matrix composite coating is mainly composed of α-Ti cellular dendrites and a eutectic in which a large number of coarse rod/needle-shaped and fine needle-shaped TiB particles and a few equiaxial TiC particles are homogeneously embedded. The microstructural evolution can be divided into four stages: $L \Leftrightarrow \beta\text{-Ti}_{\text{D}} + L_{\text{n}}$; $L_{\text{D}} \Leftrightarrow (\beta\text{-Ti} + \text{TiB})_{\text{e}} + L_{\text{e}}$; $L_{\text{e}} \Leftrightarrow \beta\text{-Ti} + \text{TiB} + \text{TiC}$; and $\beta\text{-Ti} \Leftrightarrow \alpha\text{-Ti}$. The microhardness of the coating presents a gradient variation from the surface (about HV 0.2 876) to the bottom (about HV 0.2 660), prominently improved in comparison with that of the substrate. The fracture toughness of the coating also exhibits a gradient variation from the surface (6.3 MPa•$m^{1/2}$) to the bottom (11.9 MPa•$m^{1/2}$). The coating exhibits excellent wear resistance. Scraps are mainly composed of a great amount of Fe_2O_3 and little Fe, which will shield the coating from being worn away. No titanium, TiB or TiC are present in the scraps due to the improved wear resistance of the coating.

References

[1] Y Wang, H M Wang. Wear Resistance of Laser Clad Ti_2Ni_3Si Reinforced Intermetallic Composite Coatings on Titanium Alloy [J]. *Appl. Surf. Sci.,* 2004, 229: 81-86

[2] R L Sun, D Z Yang, L X Guo, *et al*. Laser Cladding of Ti-6Al-4V Alloy with TiC and TiC+NiCrBSi Powders Surface and Coatings Technology [J]. *Surf. Coat. Technol.,* 2001, 135: 307-312

[3] M Hazra, A K Mondal, S Kumar, *et al*. Laser Surface Cladding of MRI 153M Magnesium Alloy with (Al+Al_2O_3) [J]. *Surf. Coat. Technol.,* 2009, 203: 2 292-2 299

[4] S Yang, M L Zhong, W J Liu. TiC Particulate Composite Coating Produced *in Situ* by Laser Cladding [J]. *Mater. Sci. Eng. A,* 2003, 343: 57-62

[5] X Cao, M Xiao, M Jahazi. Nd:YAG Laser Welding of Magnesium Alloy Castings [J]. *Mater. Manuf. Process.,* 2005, 20:987-1 004

[6] J A Vreeling, V Ocelik, J T M De Hosson. Ti-6Al-4V Strengthened by Laser Melt Injection of WCp Particles [J]. *Acta Mater.,* 2002, 50: 4 913-4 924

[7] Y M Zhang, M Hida, A Sakakibara, *et al*. Effect of WC Addition on Microstructures of Laser Melted Ni-based Alloy Powder [J]. *Surf. Coat. Technol.,* 2003, 169-170: 384-387

[8] J Przybylowicz, J Kusinski. Structure of Laser Cladded Tungsten Carbide Composite Coatings [J]. *J. Mater. Process. Technol.,* 2001, 109: 154-160

[9] R X Liu, T Q Lei, L X Guo. Stratification Mechanism and Interface Characterization of (TiN), (TiC)/NiCrBSi Composite Coatings Synthesized by Laser Remelting [J]. *Surf. Rev. Lett.,* 2004, 11: 291-295

[10] H C Man, S Zhang, F T Cheng, *et al*. *In Situ* Formation of a TiN/Ti Metal Matrix Composite Gradient Coating on NiTi by Laser Cladding and Nitriding [J]. *Surf. Coat. Technol.,* 2006, 200: 4 961-4 966

[11] B G Guo, J S Zhoua, S T Zhang, *et al*. Microstructure and Tribological Properties of *In Situ* Synthesized TiN/Ti_3Al Intermetallic Matrix Composite Coatings on Titanium by Laser Cladding and Laser Nitriding [J]. *Mater. Sci. Eng. A,* 2008, 480: 404-410

[12] X H Wang, M Zhang, Z D Zou, *et al*. Microstructure and Properties of Laser Clad TiC+NiCrBSi+Rare Earth Composite Coatings [J]. *Surf. Coat. Technol.,* 2002, 161: 195-199

[13] Y Chen, H M Wang. Growth Morphology and Mechanism of Primary TiC Carbide in Laser Clad TiC/FeAl Composite Coating [J]. *Mater. Lett.,* 2003, 57:1 233-1 238

[14] H C Man, S Zhang, F T Cheng, *et al*. Microstructure and Formation Mechanism of *In Situ* Synthesized TiC/Ti Surface MMC on Ti-6Al-4V by Laser Cladding [J]. *Scripta Mater.,* 2001, 44: 2 801-2 807

[15] B G Guo, J S Zhou, S T Zhang, *et al*. Phase Composition and Tribological Properties of Ti-Al Coatings Produced on Pure Ti by Laser Cladding [J]. *Appl. Surf. Sci.,* 2007, 253: 9 301-9 310

[16] B J Kooi, Y T Pei, J T M De Hosson. The Evolution of Microstructure in a Laser Clad TiB-Ti Composite Coating [J]. *Acta Mater.,* 2003, 51: 831-845

[17] R Banerjee, A Genc, D Hill, *et al*. Nanoscale TiB Precipitates in Laser Deposited Ti-Matrix Composites [J]. *Scripta Mater.,* 2005, 53: 1 433-1 437

[18] S Mridha, T N Baker. Composite Layer Formation on Ti-6AI-4V Surfaces by Laser Treatment Using Preplaced SiC Powder [J]. *Surf. Eng.*, 1997, 13: 233-237

[19] J H Ouyang, S Nowotny, A Richter, *et al*. Characterization of Laser Clad Yttria Partially-Stabilized ZrO_2 Ceramic Layers on Steel 16MnCr5 [J]. *Surf. Coat. Technol.,* 2001, 137: 12-20

[20] H M Wang, Y L Yu, S Q Li. Microstructure and Tribological Properties of Laser Clad CaF_2/Al_2O_3 Self-lubrication Wear Resistant Ceramic Matrix Composite Coatings [J]. *Scripta Mater.,* 2002, 47: 57-61

[21] B V Radhakrishna Bhat, J Subramanyam, V V Bhanu Prasad. Preparation of Ti-TiB-TiC & Ti-TiB Composites by *In Situ* Reaction Hot Pressing [J]. *Mater. Sci. Eng. A,* 2002, 325: 126-130

[22] X H Zhang, Q Xu, J C Han, *et al*. Self-propagating High Temperature Combustion Synthesis of TiB/Ti Composites [J]. *Mater. Sci. Eng. A,* 2003, 348: 41-46

[23] D Hill, R Banerjee, D Huber, *et al*. Formation of Equiaxed Alpha in TiB Reinforced Ti Alloy Composites [J]. *Scripta Mater.,* 2005, 52: 387-392

[24] Y Liu, L F Chen, H P Tang, *et al*. Design of Powder Metallurgy Titanium Alloys and Composites [J]. *Mater. Sci. Eng. A,* 2006, 418: 25-35

[25] E Zhang, G Zeng, S Y Zeng. Effect of *In Situ* TiB Short Fibre on Oxidation Behavior of Ti-6Al-1.2B Alloy [J]. *Scripta. Mater.,* 2002, 46: 811-816

[26] K Geng, W J Lu, Z F Yang, *et al*. *In Situ* Preparation of Titanium Matrix Composites Reinforced by TiB and Nd_2O_3 [J]. *Mater. Lett.,* 2003, 57: 4 054-4 057

[27] K Geng, W J Lu, Y X Qin, *et al*. *In Situ* Preparation of Titanium Matrix Composites Reinforced with TiB Whiskers and Y_2O_3 Particles [J]. *Mater. Res. Bull.,* 2004, 39: 873-879

[28] D Xu, W J Lu, Z F Yang, *et al*. *In Situ* Technique for Synthesizing Multiple Ceramic Particulates Reinforced Titanium Matrix Composites (TiB + TiC +Y_2O_3)/Ti [J]. *J. Alloy Compd.,* 2005, 400: 216-221

[29] W J Lu, D Zhang, X N Zhang, *et al*. Microstructural Characterization of TiB *In Situ* Synthesized Titanium Matrix Composites Prepared by Common Casting Technique [J]. *J. Alloy Compd.,* 2001, 327: 240-247

[30] Z F Yang, W J Lu, J N Qin, *et al*. Microstructure and Tensile Properties of *In Situ* Synthesized (TiC+TiB+Nd_2O_3)/Ti-Alloy Composites at Elevated Temperature [J]. *Mater. Sci. Eng. A,* 2006, 425: 185-191

[31] M J Mas-Guindal, L Contreras, X Turrillas. Self-Propagating High Temperature Synthesis of TiC-WC Composite Materials [J]. *J. Alloy Compd.,* 2006, 419: 227-233

[32] S Gorsse, Y L Petitcorps, S Matar, *et al*. Investigation of the Young' s Modulus of TiB Needles *In Situ* Produced in Titanium Matrix Composite [J]. *Mater. Sci. Eng. A,* 2003, 340: 80-87

[33] L F Cai, Y Z Zhang, L K Shi. Microstructure and Formation Mechanism of Titanium Matrix Composites Coating on Ti-6A1-4V by Laser Cladding [J]. *Rare Metals,* 2007, 26: 342-346

[34] D L Ye. *Practical Inorganic Thermodynamics Manual* [M]. Beijing: Metallurgy Industry Press, 2002:2-287

[35] X N Zhang, W J Lu, D Zhang, *et al*. *In Situ* Technique for Synthesizing (TiB+TiC)/Ti Composites [J]. *Scripta Mater.,* 1999, 41: 39-46

[36] W J Lu, X N Zhang, D Zhang, *et al*. Thermodynamic Research on *In Situ* Formation of TiB and Reinforced Titanium Matrix Composites [J]. *Chinese J. Nonf. Metal.,* 1999, 9: 220-224

[37] H Duschanek, P Rogal, H L Lukas. A Critical Assessment and Thermodynamic Calculation of the Boron-Carbon-Titanium (B-C-Ti) Ternary System [J]. *J. Phase Equilib.,* 1995, 16:46-60

[38] C Hu, L Barnard, S Mridha, *et al*. The Role of SiC Particulate and Al_2O_3 (Saffil) Fibers in Several Alloys during the Formation of *In Situ* MMCs Developed by Laser Processing [J]. *J. Mater. Process. Technol.,* 1996, 58: 87-95

[39] X L Wu. *In Situ* Formation by Laser Cladding of a TiC Composite Coating with a Gradient Distribution [J]. *Surf. Coat. Technol.,* 1999, 115:111-115